

Article

Thermal Stability of Ru–Al Multilayered Thin Films on Inconel 617

Yung-I Chen *, Zhi-Ting Zheng and Jia-Wei Jhang

Institute of Materials Engineering, National Taiwan Ocean University, Keelung 20224, Taiwan; 10455001@mail.ntou.edu.tw (Z.-T.Z.); 10555006@mail.ntou.edu.tw (J.-W.J.)

* Correspondence: yichen@mail.ntou.edu.tw; Tel.: +886-2-2462-2192

Received: 7 June 2018; Accepted: 2 July 2018; Published: 4 July 2018



Abstract: Ru-riched and equiatomic Ru–Al multilayered thin films were fabricated on Si and Inconel 617 substrates. These thin films exhibited a multilayered structure that is caused by stacking cyclical gradient concentration through cosputtering. X-ray diffraction analysis indicated that the as-deposited Ru–Al multilayers comprised Ru and RuAl phases. Oxidation that is caused by annealing atmospheres and elements diffused from substrates was investigated. The results indicated that the inward diffusion of O at 600 °C in a 1% O₂–99% Ar atmosphere was restricted by the formation of an amorphous Al-oxide sublayer, and inward diffusion of O at 800 °C in air was limited by the formation of a crystalline Al₂O₃ scale. Additionally, the outward diffusion of elements from Inconel 617 penetrated the unoxidized parts of the 800 °C–annealed Ru–Al multilayers.

Keywords: multilayer; oxidation; RuAl; thermal stability

1. Introduction

Inconel 617, which is a Ni-based superalloy, is widely used in metal components that must withstand temperatures above 800 °C [1,2]. Thermal barrier coatings (TBCs) are employed for high-temperature applications to provide thermal and oxidation protection to metal components [3,4]. Y₂O₃-stabilized ZrO₂ (YSZ) has been used as a TBC for gas turbine blades and vanes [5–9]. Because O can penetrate YSZ, aluminide bond coats (BCs) have been used to combine YSZ and Ni-based superalloys. These BCs behave as diffusion barriers after forming thermally grown oxides (TGO), such as α -Al₂O₃. Therefore, a typical TBC/TGO/BC/superalloy assembly is a common material structure in jet engine components. RuAl exhibits excellent oxidation resistance, thermodynamic stability, and strength at high temperatures, as well as excellent ductility at room temperature [10,11]. Moreover, RuAl and Al₂O₃ possess similar coefficients of thermal expansion [12]. Accordingly, Ru-modified aluminides have been used as BCs for thermal barrier systems [13,14]. RuAl thin films that were fabricated by sputtering have also been considered for use as working layers for glass molding dies at temperatures above 600 °C [15,16] and for metallization on surface acoustic wave devices that are annealed at 800 °C under high vacuum conditions [17–20]. Therefore, it is important to understand the thermal stability of Ru–Al thin films at high temperatures. In a previous study [21], the oxidation behavior of Ru_{0.63}Al_{0.37} multilayered thin films prepared on Si substrates was investigated in a low-oxygen-content atmosphere of 1% O₂–99% Ar, and the films exhibited internal and external oxidation at 400–600 and 700–800 °C, respectively. A 1% O₂–99% Ar atmosphere has also been used as an oxidation-accelerating atmosphere to evaluate the performance of protective coatings on glass molding dies [22]. In the present study, the oxidation resistance of Ru_{0.48}Al_{0.52} multilayered thin films in 1% O₂–99% Ar atmosphere at 600 °C was evaluated. Subsequently, the thermal stability of the Ru_{0.63}Al_{0.37} and Ru_{0.48}Al_{0.52} thin films that were prepared on Inconel 617 substrates in air at 800 °C was investigated.

2. Materials and Methods

Ru–Al multilayered thin films with an interlayer were fabricated through magnetron cosputtering onto silicon and Inconel 617 substrates with dimensions of $20 \times 20 \times 0.525 \text{ mm}^3$ and $20 \times 20 \times 3 \text{ mm}^3$, respectively. Ti and Ru interlayers were deposited to improve the adhesion strength of Ru–Al thin films on Si and Inconel 617 substrates, respectively. Pure metal targets of Ru (99.95%), Al (99.999%), and Ti (99.995%) with diameters of 50.8 mm each were adopted as source materials for sputtering (Figure 1). The sputter guns were inclined to focus plasma on the circular track of the substrate holder, which resulted in cyclical gradient concentration deposition [21,23,24]. The cosputtering processes for fabricating multilayered thin films were described in detail in a previous study [23]. Ru and Al were cosputtered onto the interlayers using various powers, while the substrate holder was rotated at 1 rpm and kept at $400 \text{ }^\circ\text{C}$ during sputtering. After sputtering Ru–Al deposits for 35 min, the sputter power of Al target was turned off for an extra substrate holder revolution to fabricate a Ru layer on the surface for protective purposes [21]. The Ru–Al thin films that were deposited on Si and Inconel 617 were further annealed at $600 \text{ }^\circ\text{C}$ in 1% O_2 –99% Ar and at $800 \text{ }^\circ\text{C}$ in air, respectively.

Chemical composition analyses were conducted using a field emission electron probe microanalyzer (FE-EPMA, JXA-8500F, JEOL, Akishima, Japan) at a 12-kV accelerating voltage on the surface. Surface morphology and thickness measurement of the thin films were performed by using a field emission scanning electron microscope (FE-SEM, S4800, Hitachi, Tokyo, Japan) at a 15-kV accelerating voltage. A conventional X-ray diffractometer (XRD, X'Pert PRO MPD, PANalytical, Almelo, The Netherlands) with Cu $K\alpha$ radiation was used to identify the thin film phases using a grazing incidence technique at an incidence angle of 1° . The accelerating voltage and the current of XRD in this study were applied for 45 kV and 40 mA, respectively. The nanostructure of the thin films and scales was further examined using transmission electron microscopy (TEM, JEM-2010F, JEOL, Tokyo, Japan) at a 200-kV accelerating voltage. TEM samples were prepared by applying a focused ion beam system (FEI Nova 200, Hillsboro, OR, USA) at an accelerating voltage of 30 kV with a gallium ion source. A Pt layer was deposited to protect the free surface during sample preparation. An energy dispersive spectrometry (EDS, Inca x-sight, Oxford Instruments, Tokyo, Japan), equipped with the TEM was used to determine local chemical compositions qualitatively. The residual stress of the films prepared on Si substrates, as measured by the curvature method was calculated using Stoney's equation [25].

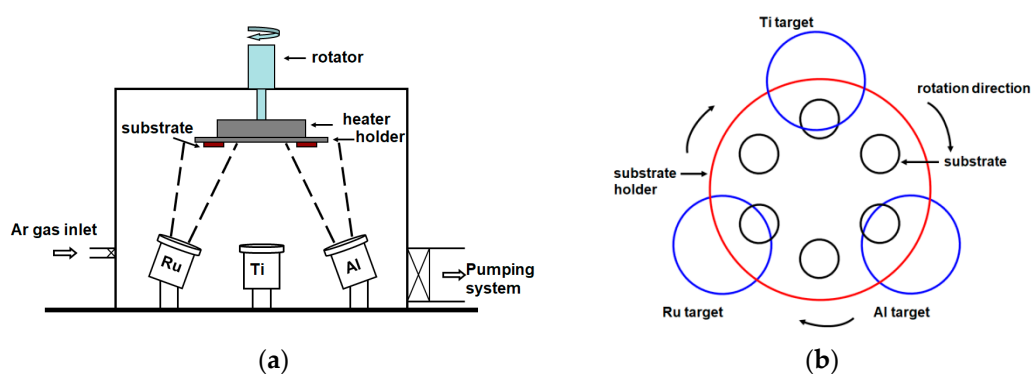


Figure 1. (a) Schematic of the cosputtering equipment and (b) substrate holder and sample positions related to sputter targets.

3. Results and Discussion

3.1. As-Deposited Ru–Al Thin Films

Table 1 lists the chemical compositions of the as-deposited Ru–Al thin films that were prepared on Si substrates using various sputter powers and a substrate holder rotation speed of 1 rpm. The thin films are denoted in the table as $\text{Ru}_{0.89}\text{Al}_{0.11}$, $\text{Ru}_{0.63}\text{Al}_{0.37}$, and $\text{Ru}_{0.48}\text{Al}_{0.52}$. Figure 2 presents the XRD patterns of the as-deposited Ru–Al thin films. The $\text{Ru}_{0.89}\text{Al}_{0.11}$ thin films exhibited a hexagonal Ru [ICDD 00-006-0663] phase, whereas the $\text{Ru}_{0.63}\text{Al}_{0.37}$ and $\text{Ru}_{0.48}\text{Al}_{0.52}$ thin films exhibited a mixture of cubic RuAl [ICDD 00-029-1404] and Ru phases. The peaks at the two-theta angle of approximately 52° were caused by the Si substrate [26]. The reflections of the Ti interlayers were not observed because they were of low intensity. Figure 3 depicts the XRD pattern of the $\text{Ru}_{0.48}\text{Al}_{0.52}/\text{Ti}/\text{Si}$ samples that were captured using a Bragg–Brentano scan. The scan indicated RuAl and Ru phases accompanied by a Ti phase. Figure 4 presents a cross-sectional SEM image of the as-deposited $\text{Ru}_{0.48}\text{Al}_{0.52}$ thin films. The films exhibited a columnar and multilayered structure due to cyclical gradient concentration deposition. The thickness of the $\text{Ru}_{0.48}\text{Al}_{0.52}$ thin film was 1083 nm. Because the number of revolutions of the substrate holder was 35, the multilayered structure of the $\text{Ru}_{0.48}\text{Al}_{0.52}$ thin film had a stacking period of 31 nm. The $\text{Ru}_{0.89}\text{Al}_{0.11}$ and $\text{Ru}_{0.63}\text{Al}_{0.37}$ thin films both exhibited stacking periods of 37 nm (Table 1).

Table 1. Chemical compositions, thicknesses, and stacking periods of the as-deposited Ru–Al thin films.

Sample	Sputter Power (W)		Chemical Composition (at.%)			Thickness (nm)		Period (nm)
	W_{Ru}	W_{Al}	Ru	Al	O	Film	Interlayer	
$\text{Ru}_{0.89}\text{Al}_{0.11}$	200	100	86.69 ± 0.39	10.89 ± 0.02	2.42 ± 0.37	1305	50	37
$\text{Ru}_{0.63}\text{Al}_{0.37}$	150	150	59.33 ± 0.32	34.75 ± 0.32	5.92 ± 0.03	1312	50	37
$\text{Ru}_{0.48}\text{Al}_{0.52}$	100	200	47.35 ± 0.39	52.06 ± 0.34	0.59 ± 0.14	1083	50	31

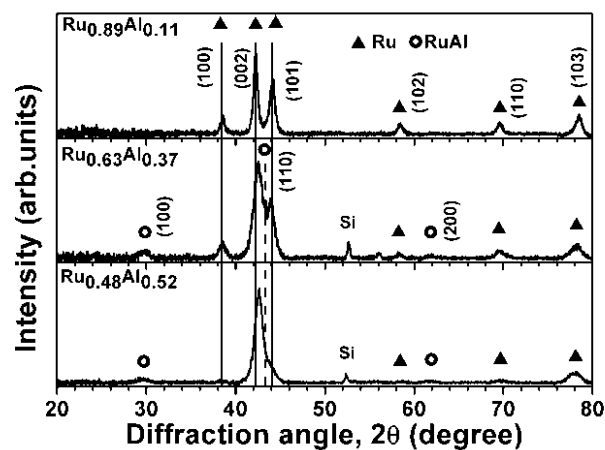


Figure 2. X-ray diffractometer (XRD) patterns of as-deposited Ru–Al thin films.

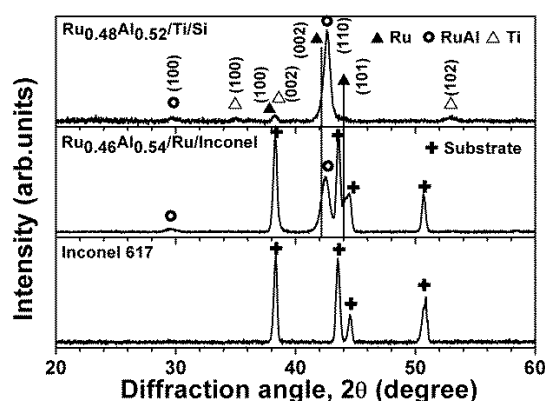


Figure 3. Bragg–Brentano scan of XRD patterns from the Inconel substrate, $\text{Ru}_{0.46}\text{Al}_{0.54}/\text{Ru}/\text{Inconel}$, and $\text{Ru}_{0.48}\text{Al}_{0.52}/\text{Ti}/\text{Si}$ samples.

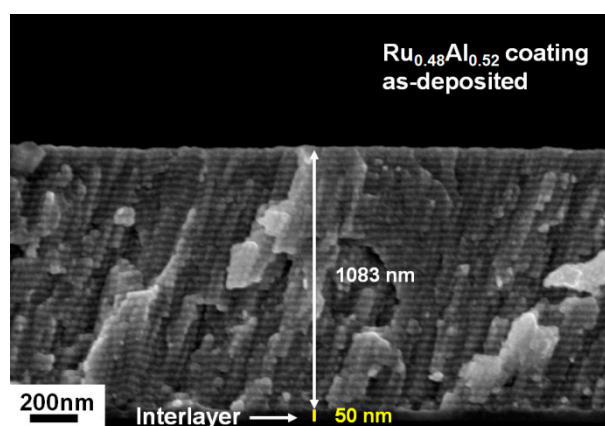


Figure 4. Cross-sectional SEM image of the as-deposited $\text{Ru}_{0.48}\text{Al}_{0.52}$ thin films.

3.2. $\text{Ru}_{0.48}\text{Al}_{0.52}$ Thin Films Annealed in 1% O_2 –99% Ar at 600 °C

Figure 5 presents a cross-sectional SEM image of the $\text{Ru}_{0.48}\text{Al}_{0.52}$ thin films that were annealed in 1% O_2 –99% Ar at 600 °C for 24 h. The surface oxide scales were not evident and the laminated layers were maintained. The thickness of the films increased slightly from 1083 to 1102 nm, whereas the Ti interlayer increased from 50 to 151 nm, implying the interdiffusion of Ti and Si. Figure 6 exhibits the XRD patterns of the annealed $\text{Ru}_{0.48}\text{Al}_{0.52}$ thin films. RuO_2 reflections [ICDD 00-040-1290] were observed after annealing for 30 min. Ru and RuAl phases were observed even after annealing for up to 24 h. Figure 7a exhibits the cross-sectional TEM image of the 24 h-annealed $\text{Ru}_{0.48}\text{Al}_{0.52}$ thin films, in which the multilayered structure was maintained. The EDS results qualitatively indicated that the surface scale was Al-oxide (Position 1), and the O content exhibited a higher level of 14–25 at.% for the first stacking periods (Positions 2 and 3). The columnar structure had a width of 50 nm. The original Ru toplayer disappeared; this may be attributed to the oxidation of Ru to the higher valance states of RuO_3 or RuO_4 , which are volatile [20,27,28]. Because the standard Gibbs free energies of RuO_3 and RuO_4 at 600 °C are -16.908 and -28.003 kJ/(mol of O_2) [29], respectively, and the atmosphere was constructed by constantly flowing O_2 –Ar mixed gases into a tube furnace, the formation of these volatile oxides was possible. In a previous study [22], partial Re atoms in IrRe films formed volatile Re_2O_7 and escaped after annealing in 1% O_2 –99% Ar at 600 °C for 500 min. The EDS results also indicated that Positions 5 and 7 were Ru-enriched black sublayers, whereas Positions 4, 6, and 8 were Al-enriched gray sublayers. The columnar boundaries may have provided oxygen diffusion paths [21,30] in the early oxidation stage. High-resolution TEM imaging indicated that the surface

Al-oxide scale was amorphous, and the lattice fringes of RuO₂ were observed beneath the surface oxide layer (Figure 7b). The amorphous Al-oxide sublayer restricted oxidation at 600 °C in 1% O₂–99% Ar. The oxidation of the Ru_{0.48}Al_{0.52} thin films at 600 °C in 1% O₂–99% Ar was similar to that of the Ru_{0.63}Al_{0.37} thin films that were reported previously [21]. The oxidation depth of Ru_{0.63}Al_{0.37} thin films after annealing for 24 h was approximately the outmost two stacking periods. By contrast, the Ru_{0.89}Al_{0.11} thin films detached after they were annealed in 1% O₂–99% Ar at 600 °C for 30 min. Because the as-deposited Ru_{0.89}Al_{0.11}, Ru_{0.63}Al_{0.37}, and Ru_{0.48}Al_{0.52} thin films exhibited similar residual stress levels of 1.57 ± 0.16 , 1.43 ± 0.16 , and 1.61 ± 0.29 GPa, respectively, the detachment of the Ru_{0.89}Al_{0.11} films was attributed to a high oxide–metal–volume ratio of 2.32 for RuO₂/Ru. This value was determined using an XRD database.

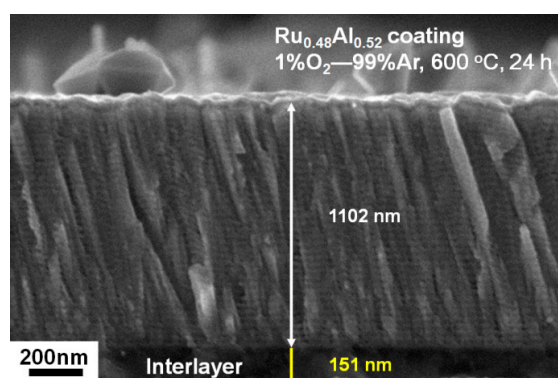


Figure 5. Cross-sectional SEM image of the Ru_{0.48}Al_{0.52} thin films annealed in 1% O₂–99% Ar at 600 °C for 24 h.

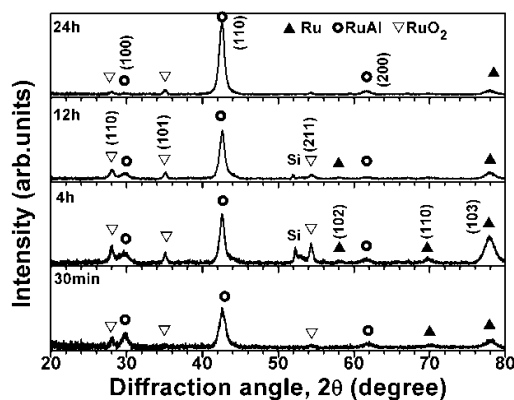


Figure 6. XRD patterns of the Ru_{0.48}Al_{0.52} thin films annealed in 1% O₂–99% Ar at 600 °C for 0.5–24 h.

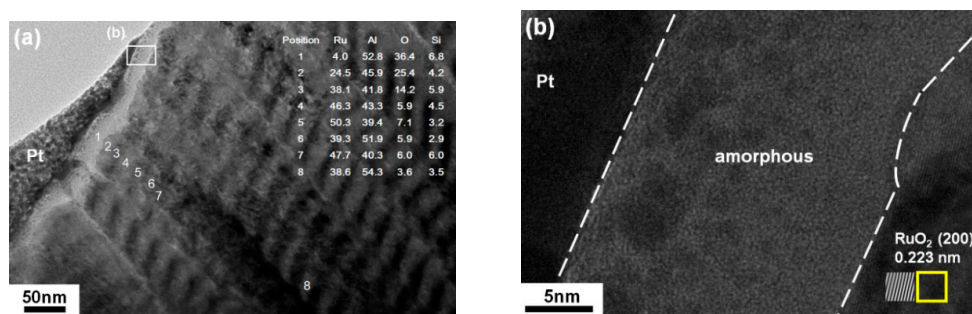


Figure 7. (a) Cross-sectional transmission electron microscopy (TEM) image and (b) high-resolution TEM image of the Ru_{0.48}Al_{0.52} thin films annealed in 1% O₂–99% Ar at 600 °C for 24 h.

3.3. Ru–Al Thin Films Annealed in Air at 800 °C

Table 2 presents the chemical compositions of the Ru–Al thin films deposited on Inconel 617 substrates with a Ru interlayer. These thin films were denoted as Ru_{0.81}Al_{0.19}, Ru_{0.61}Al_{0.39}, and Ru_{0.46}Al_{0.54}. Figure 8 depicts XRD patterns of the Ru–Al thin films that were prepared on Inconel 617 substrates with a Ru interlayer. These patterns were similar to those of the Ru–Al thin films prepared on Si substrates with a Ti interlayer (Figure 2). The Ru_{0.81}Al_{0.19} thin films exhibited a Ru phase, and the Ru_{0.61}Al_{0.39} and Ru_{0.46}Al_{0.54} thin films exhibited a mixture of RuAl and Ru phases. Because both the Ti and Ru interlayers have hexagonal phases, the crystalline phases of Ru–Al thin films deposited on the two interlayers were the same. The reflections of the Inconel 617 substrates were not observed due to low intensity and overlapping with reflections of Ru and RuAl phases. The XRD patterns of an Inconel 617 substrate and the Ru_{0.46}Al_{0.54}/Ru/Inconel samples under a Bragg–Brentano scan are presented in Figure 3. Figure 9 exhibits the XRD patterns of the Ru–Al thin films after they were annealed in air at 800 °C for 30 min. Ru and RuO₂ dominated the crystalline phases, whereas RuAl became a minor phase. No Al₂O₃ reflections were evident; however, Al should be preferentially oxidized, implying that the Al-oxide should be X-ray amorphous. Part of the annealed Ru_{0.81}Al_{0.19} thin films detached after annealing. This phenomenon was similar to that of the 1% O₂–99% Ar, 600 °C, and 30 min-annealed Ru_{0.89}Al_{0.11} thin films prepared on Si substrates. Figure 10 illustrates the surface morphologies of the Ru_{0.61}Al_{0.39} and Ru_{0.46}Al_{0.54} thin films after they were annealed in air at 800 °C for 30 min. No spallation was evident, but cracks and small granular oxide particles were observed on the surface of the annealed Ru_{0.61}Al_{0.39} films, whereas the annealed Ru_{0.46}Al_{0.54} films only exhibited oxide particles.

Table 2. Chemical compositions of Ru–Al thin films deposited on Inconel 617 with a Ru interlayer.

Sample	Sputter Power (W)		Chemical Composition (at.%)		
	W _{Ru}	W _{Al}	Ru	Al	O
as-deposited					
Ru _{0.81} Al _{0.19}	200	100	80.02 ± 0.58	19.16 ± 0.24	0.82 ± 0.78
Ru _{0.61} Al _{0.39}	150	150	57.16 ± 0.20	37.16 ± 0.06	5.68 ± 0.15
Ru _{0.46} Al _{0.54}	100	200	44.80 ± 0.03	52.54 ± 0.15	2.66 ± 0.13

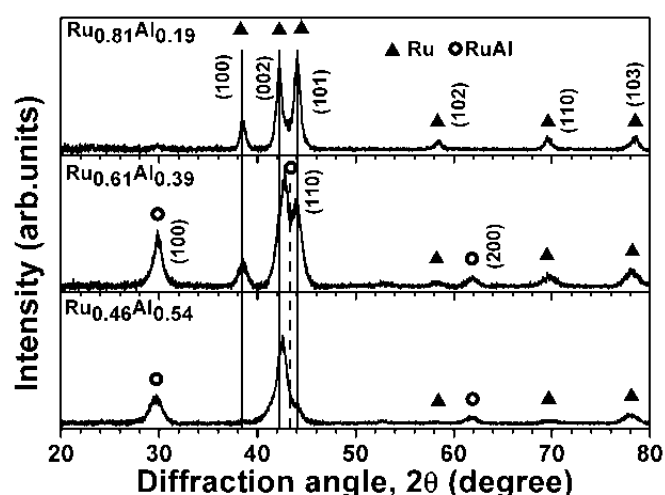


Figure 8. XRD patterns of the as-deposited Ru–Al thin films prepared on Inconel 617 substrates with a Ru interlayer.

surrounding Position 6 thickened, which was attributed to the outward diffusion of Ni, Cr, and Co from Inconel 617, as identified by EDS.

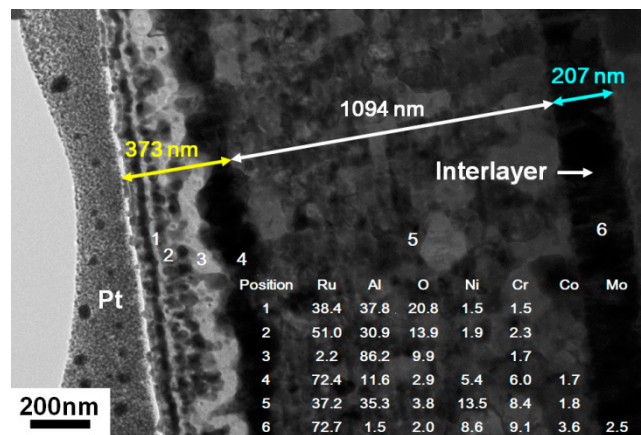


Figure 11. Cross-sectional TEM image and energy dispersive spectrometry (EDS) results for the $\text{Ru}_{0.61}\text{Al}_{0.39}/\text{Ru}/\text{Inconel 617}$ sample after annealing in air at $800\text{ }^\circ\text{C}$ for 30 min.

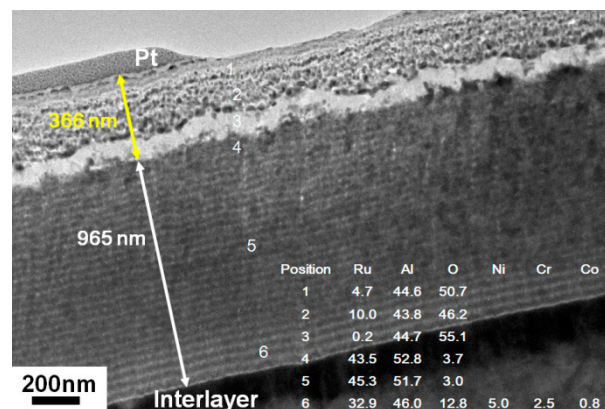


Figure 12. Cross-sectional TEM image and EDS results for the $\text{Ru}_{0.46}\text{Al}_{0.54}/\text{Ru}/\text{Inconel 617}$ sample after annealing in air at $800\text{ }^\circ\text{C}$ for 30 min.

Figure 13 presents the XRD patterns of the $\text{Ru}_{0.46}\text{Al}_{0.54}/\text{Ru}/\text{Inconel 617}$ sample after annealing in air at $800\text{ }^\circ\text{C}$ for 4 h. The patterns exhibited reflections of RuAl, RuO_2 , $\gamma\text{-Al}_2\text{O}_3$ [ICDD 00-050-0741], and $\alpha\text{-Al}_2\text{O}_3$ [ICDD 00-046-1212] phases. Figure 14a depicts the cross-sectional TEM image of the $\text{Ru}_{0.46}\text{Al}_{0.54}$ thin films after annealing in air at $800\text{ }^\circ\text{C}$ for 4 h; this image exhibited an oxide scale of 140 nm and an inner part of 1345 nm. The inner part comprised an interdiffused film, interlayer, and substrate. The oxide scale exhibited a high O level of 45 at.% at Position 1, for which a high-resolution TEM image exhibited lattice fringes of crystalline $\alpha\text{-Al}_2\text{O}_3$ (Figure 14b). The depth of the oxide scale of the 4 h-annealed $\text{Ru}_{0.46}\text{Al}_{0.54}$ thin films appeared to be less than that of the 30 min-annealed films (Figure 12), which implied that the outmost oxidized part of the films volatilized during further oxidation, and only the Al_2O_3 -dominant oxide scale remained. Figure 14c represents the RuAl grains of 200 nm that were beneath the oxide scale.

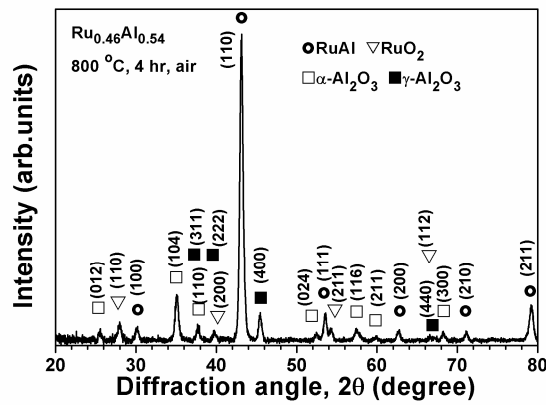


Figure 13. XRD pattern of the Ru_{0.46}Al_{0.54}/Ru/Inconel 617 sample after annealing in air at 800 °C for 4 h.

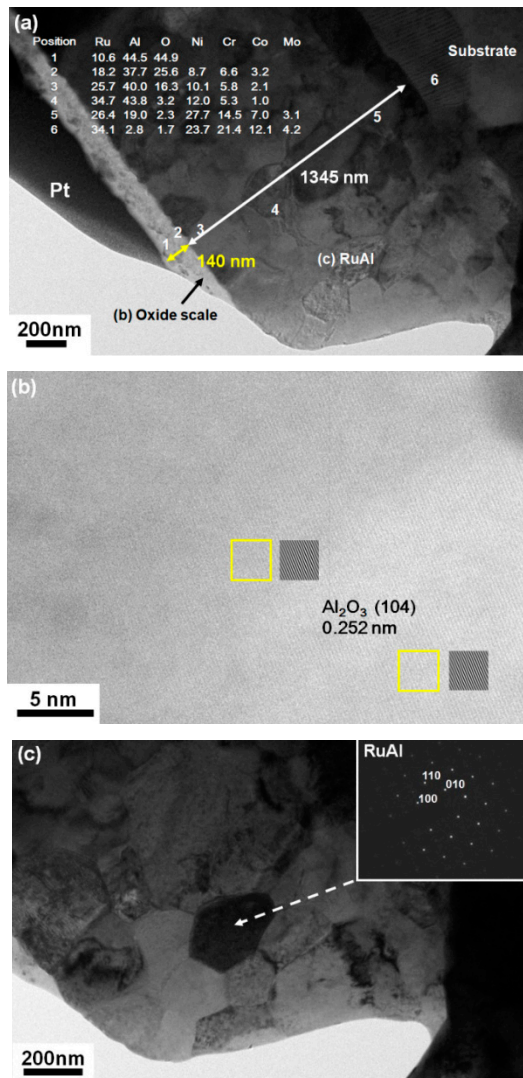


Figure 14. (a) Cross-sectional TEM image of the Ru_{0.46}Al_{0.54} thin films annealed in air at 800 °C for 4 h, (b) high-resolution TEM image of the surface oxide scale, and (c) a RuAl grain beneath the oxide scale.

4. Conclusions

Ru–Al multilayered thin films that were stacked with cyclical gradient concentration were fabricated through cosputtering. The oxidation depth of Ru_{0.48}Al_{0.52} thin films that were annealed in a 1% O₂–99% Ar atmosphere at 600 °C for 24 h was restricted at the outmost two stacking periods, which behaved similar to that of the Ru_{0.63}Al_{0.37} thin films and was attributed to the formation of amorphous Al-oxide sublayers restricting the inward diffusion of O. Additionally, the oxidation fronts to five stacking periods of the Ru_{0.46}Al_{0.54} and Ru_{0.61}Al_{0.39} thin films after they were annealed in air at 800 °C for 30 min. The Al-oxide sublayers remained amorphous. In the interior part of the Ru_{0.61}Al_{0.39} films, (i.e., the unoxidized portions) the multilayered structure transformed into large grains, accompanied by outward diffusion of Inconel 617 substrate elements. By contrast, the unoxidized part of the Ru_{0.46}Al_{0.54} films maintained its multilayer structure after 30 min of annealing, and the diffusion of elements from the substrate was limited. An extending annealing time of 4 h resulted in the formation of a crystalline α -Al₂O₃-dominated oxide scale on the surface of the Ru_{0.46}Al_{0.54} films, and the original Ru on the surface region formed volatile oxides. Additionally, beneath the α -Al₂O₃ oxide scale, the structure transformed into large grains of RuAl phase accompanied by the outward diffusion of substrate elements. Modification of the Ru–Al multilayered thin films by introducing a third element to form a diffusion barrier for constitutive elements of Inconel 617 is a major concern that should be addressed in future research.

Author Contributions: Conceptualization, Project Administration, and Writing—Original Draft Preparation, Y.-I.C.; Investigation, Z.-T.Z. and J.-W.J.

Funding: This research was funded by the Ministry of Science and Technology, Taiwan. The grant number is 106-2221-E-019-022-MY3.

Acknowledgments: The support of Inconel 617 materials from Wu Kai at National Taiwan Ocean University is greatly acknowledged.

Conflicts of Interest: The authors declare no conflict of interest.

References

1. Rahman, M.d.S.; Priyadarshan, G.; Raja, K.S.; Nesbitt, C.; Misra, M. Characterization of high temperature deformation behavior of INCONEL 617. *Mech. Mater.* **2009**, *41*, 261–270. [[CrossRef](#)]
2. Gariboldi, E.; Cabibbo, M.; Spigarelli, S.; Ripamonti, D. Investigation on precipitation phenomena of Ni–22Cr–12Co–9Mo alloy aged and crept at high temperature. *Int. J. Press. Vessel. Pip.* **2008**, *85*, 63–71. [[CrossRef](#)]
3. DeMasi-Marcin, J.T.; Gupta, D.K. Protective coatings in the gas turbine engine. *Surf. Coat. Technol.* **1994**, *68–69*, 1–9. [[CrossRef](#)]
4. Vaßen, R.; Jarligo, M.O.; Steinke, T.; Mack, D.E.; Stöver, D. Overview on advanced thermal barrier coatings. *Surf. Coat. Technol.* **2010**, *205*, 938–942. [[CrossRef](#)]
5. Miller, R.A. Current status of thermal barrier coatings—An overview. *Surf. Coat. Technol.* **1987**, *30*, 1–11. [[CrossRef](#)]
6. Evans, A.G.; Mumm, D.R.; Hutchinson, J.W.; Meier, G.H.; Pettit, F.S. Mechanisms controlling the durability of thermal barrier coatings. *Prog. Mater. Sci.* **2001**, *46*, 505–553. [[CrossRef](#)]
7. Aygun, A.; Vasiliev, A.L.; Padture, N.P.; Ma, X. Novel thermal barrier coatings that are resistant to high-temperature attack by glassy deposits. *Acta Mater.* **2007**, *55*, 6734–6745. [[CrossRef](#)]
8. Huang, J.; Wang, W.; Lu, X.; Hu, D.; Feng, Z.; Guo, T. Effect of particle size on the thermal shock resistance of plasma-sprayed YSZ coatings. *Coatings* **2017**, *7*, 150. [[CrossRef](#)]
9. Hu, N.; Khan, M.; Wang, Y.; Song, X.; Lin, C.; Chang, C.; Zeng, Y. Effect of Microstructure on the Thermal Conductivity of Plasma Sprayed Y₂O₃ Stabilized Zirconia (8% YSZ). *Coatings* **2017**, *7*, 198. [[CrossRef](#)]
10. Mücklich, F.; Ilić, N. RuAl and its alloys. Part I. Structure physical properties, microstructure and processing. *Intermetallics* **2005**, *13*, 5–21. [[CrossRef](#)]
11. Mücklich, F.; Ilić, N.; Wol, K. RuAl and its alloys, part II: Mechanical properties, environmental resistance and applications. *Intermetallics* **2008**, *16*, 593–608. [[CrossRef](#)]

12. Tryon, B.; Pollock, T.M.; Gigliotti, M.F.X.; Hemker, K. Thermal expansion behavior of ruthenium aluminides. *Scr. Mater.* **2014**, *50*, 845–848. [[CrossRef](#)]
13. Tryon, B.; Feng, Q.; Wellman, R.G.; Murphy, K.S.; Yang, J.; Levi, C.G.; Nicholls, J.R.; Pollock, T.M. Multilayered ruthenium-modified bond coats for thermal barrier coatings. *Metall. Mater. Trans. A* **2006**, *37A*, 3347–3358. [[CrossRef](#)]
14. Wang, Y.; Guo, H.B.; Peng, H.; Peng, L.Q.; Gong, S.K. Diffusion barrier behaviors of (Ru,Ni)Al/NiAl coatings on Ni-based superalloy substrate. *Intermetallics* **2011**, *19*, 191–195. [[CrossRef](#)]
15. Guitar, M.A.; Woll, K.; Ramos-Moore, E.; Mücklich, F. Study of grain growth and thermal stability of nanocrystalline RuAl thin films deposited by magnetron sputtering. *Thin Solid Films* **2013**, *527*, 1–8. [[CrossRef](#)]
16. Guitar, M.A.; Ramos-Moore, E.; Mücklich, F. The influence of impurities on the formation of protective aluminum oxides on RuAl thin films. *J. Alloys Compd.* **2014**, *594*, 165–170. [[CrossRef](#)]
17. Seifert, M.; Menzel, S.B.; Rane, G.K.; Hoffmann, M.; Gemming, T. RuAl thin films on high-temperature piezoelectric substrates. *Mater. Res. Express* **2015**, *2*, 085001. [[CrossRef](#)]
18. Seifert, M.; Rane, G.K.; Menzel, S.B.; Gemming, T. TEM studies on the changes of the composition in LGS and CTGS substrates covered with a RuAl metallization and on the phase formation within the RuAl film after heat treatment at 600 and 800 °C. *J. Alloys Compd.* **2016**, *664*, 510–517. [[CrossRef](#)]
19. Seifert, M.; Rane, G.K.; Menzel, S.B.; Gemming, T. The influence of barrier layers (SiO₂, Al₂O₃, W) on the phase formation and stability of RuAl thin films on LGS and CTGS substrates for surface acoustic wave technology. *J. Alloys Compd.* **2016**, *688*, 228–240. [[CrossRef](#)]
20. Seifert, M.; Rane, G.K.; Oswald, S.; Menzel, S.B.; Gemming, T. The influence of the composition of Ru_{100-x}Al_x (x = 50, 55, 60, 67) thin films on their thermal stability. *Materials* **2017**, *10*, 277. [[CrossRef](#)] [[PubMed](#)]
21. Chen, Y.I.; Zheng, Z.T.; Kai, W.; Huang, Y.R. Oxidation behavior of Ru–Al multilayer coatings. *Appl. Surf. Sci.* **2017**, *406*, 1–7. [[CrossRef](#)]
22. Liu, S.C.; Chen, Y.I.; Tsai, H.Y.; Lin, K.C.; Chen, Y.H. Thermal stability of Ir–Re coatings annealed in oxygen-containing atmospheres. *Surf. Coat. Technol.* **2013**, *237*, 105–111. [[CrossRef](#)]
23. Chen, Y.I. Laminated structure in internally oxidized Ru–Ta coatings. *Thin Solid Films* **2012**, *524*, 205–210. [[CrossRef](#)]
24. Chen, Y.I.; Lu, T.S.; Zheng, Z.T. Internally oxidized Ru–Zr multilayer coatings. *Coatings* **2017**, *7*, 46. [[CrossRef](#)]
25. Janssen, G.C.A.M.; Abdalla, M.M.; van Keulen, F.; Pujada, B.R.; van Venrooy, B. Celebrating the 100th anniversary of the Stoney equation for film stress: Developments from polycrystalline steel strips to single crystal silicon wafers. *Thin Solid Films* **2009**, *517*, 1858–1867. [[CrossRef](#)]
26. Deng, Y.L.; Lee, J.W.; Lou, B.S.; Duh, J.G.; Chu, J.P.; Jang, J.S.C. The fabrication and property evaluation of Zr–Ti–B–Si thin film metallic glass materials. *Surf. Coat. Technol.* **2014**, *259*, 115–122. [[CrossRef](#)]
27. Bell, W.E.; Tagami, M. High-temperature chemistry of the ruthenium–oxygen system. *J. Phys. Chem.* **1963**, *67*, 2432–2436. [[CrossRef](#)]
28. Huang, J.H.; Chen, J.S. Material characteristics and electrical property of reactively sputtered RuO thin films. *Thin Solid Films* **2001**, *382*, 139–145. [[CrossRef](#)]
29. Barin, I. *Thermochemical Data of Pure Substances*, 3rd ed.; VCH: New York, NY, USA, 1995.
30. Chen, Y.I.; Chu, H.N.; Kai, W. Internal oxidation of laminated Nb–Ru coatings. *Appl. Surf. Sci.* **2016**, *389*, 477–483. [[CrossRef](#)]
31. Bellina, P.J.; Catanoiu, A.; Morales, F.M.; Rühle, M. Formation of discontinuous Al₂O₃ layers during high-temperature oxidation of RuAl alloys. *J. Mater. Res.* **2006**, *21*, 276–286. [[CrossRef](#)]
32. Soldera, F.; Ilić, N.; Brännström, S.; Barrientos, I.; Gobran, H.; Mücklich, F. Formation of Al₂O₃ scales on single-phase RuAl produced by reactive sintering. *Oxid. Met.* **2003**, *59*, 529–542. [[CrossRef](#)]

